

Effect of interfacial slip on the thin film drainage time for two equal-sized, surfactant-free drops undergoing a head-on collision: A scaling analysis

A. Ramachandran¹ and L. G. Leal²

¹*Department of Chemical Engineering & Applied Chemistry, University of Toronto, Toronto, Ontario, Canada M5S 3E5*

²*Department of Chemical Engineering, University of California, Santa Barbara, Santa Barbara, California 93106, USA*

(Received 21 January 2016; published 21 October 2016)

Using a scaling analysis, we assess the impact of interfacial slip on the time required for the thin liquid film between two drops undergoing a head-on collision to drain to the critical thickness for rupture by van der Waals forces. Interfacial slip is included in our continuum development using a Navier slip boundary condition, with the slip coefficient modeled using previous theories [Helfand and Tagami, *J. Chem. Phys.* **57**, 1812 (1972); Goveas and Fredrickson, *Eur. Phys. J. B* **2**, 79 (1998)]. Slip decreases hydrodynamic resistance and speeds up film drainage. It renders the dependence of the drainage time on capillary number stronger in the spherical-film regime, but, interestingly, this dependence is altered only weakly in the dimpled-film regime. A subtle effect of slip is that it increases the range of capillary numbers in which the film remains predominantly spherical in shape during drainage (as opposed to being dimpled), leading to significantly faster drainage for these capillary numbers. Slip also leads to an increase in the critical capillary number beyond which coalescence is not possible in a head-collision.

DOI: [10.1103/PhysRevFluids.1.064204](https://doi.org/10.1103/PhysRevFluids.1.064204)

I. INTRODUCTION

When two polymers are blended together to form an emulsion, the droplet size distribution is the result of a subtle balance between flow-induced drop breakup events and droplet-droplet coalescence events. Although the drop-breakup phenomenon has been investigated quite extensively both experimentally and theoretically, coalescence is still poorly understood. In fact, the prediction of the rate of coalescence for even a simple situation such as the head-on collision of two equal-sized surfactant-free drops, the topic of this paper, has resisted a complete theoretical framework for prediction. This is because flow-induced coalescence is a complex process that involves several steps. First, the interfaces of the colliding drops must approach each other by squeezing out the thin film of the suspending liquid in between them, a process called hydrodynamic drainage. When the film thickness falls below a critical value, attractive forces such as van der Waals interactions manifest themselves, which destabilizes the thin film. Finally, the interfaces merge due to the formation of a hole or bridge, which opens out, and the single, large drop relaxes to a spherical shape to complete the coalescence process. The time to coalescence is the sum of the times required for each step. For small viscous drops, the rate-determining step for coalescence is hydrodynamic film drainage.

Significant effort has therefore been expended to understand the time scale for film drainage, including experimental studies [1–4], numerical simulations [5,6], and scaling theory [5–8]. A commonly used basis to compare time scales for film drainage for two equal-sized drops is to use a drainage time t_d , defined as the time increment between the moment when the center-to-center distance between the drops is $2R$ and the instant when the film ruptures. *Scaling* theory shows that the drainage time in a head-on collision between two equal-sized drops in a compressional flow should scale as $t_d G \propto Ca^m$, where G is the strain rate of the compressional flow and Ca is the capillary number, defined as

$$Ca = \frac{\mu GR}{\gamma}, \quad (1.1)$$

where R is the undeformed drop radius, γ is the interfacial tension, and μ is the viscosity of the suspending fluid. The power m depends on the shape of the thin film. A simple scaling theory that assumes a flat film for drainage of the fluid based on the analysis of Chesters [5,6] suggests that the drainage time should scale as

$$t_d G \propto \text{Ca}^{4/3}. \quad (1.2)$$

Although the scaling analysis of film drainage has been recently modified to incorporate a dimpled-film shape instead of a flat film [7], the predicted scaling of drainage time with Ca remains the same. On the other hand, if the film shape is spherical (i.e., the minimum film thickness occurs on the line of centers), a modification of the same scaling theory then suggests that the drainage time should scale as

$$t_d G \propto \text{Ca}. \quad (1.3)$$

These predictions have been tested via the numerical simulations cited above. However, the situation is a little more complicated than it might at first seem. The early stage of film drainage always occurs with the film having a spherical shape, with an initial film thickness $h_0/R \sim \beta_1 \text{Ca}$ [3]. The fact that h_0 is nonzero is a consequence of the deformation of the individual drops in the flow. However, the film continues to thin, and if it does not rupture first, there is a smaller film thickness $h_{\text{trans}}/R \sim \beta_2 \text{Ca}$ when the film undergoes a transition from spherical to the dimpled shape due to hydrodynamic interaction between the drops. The constant β_1 was shown numerically to be $O(10)$, while β_2 was found to be $O(1)$ [5]. It is then clear that the observable scaling for the drainage time will depend on whether most of the drainage process occurs before the transformation to a dimpled shape or after. This depends on the critical film thickness at the point of rupture.

In all of the numerical studies and also the experimental systems, film rupture at coalescence is due to van der Waals attraction. The critical film thickness for rupture h_{crit} has been shown in previous works to depend on both the shape of the film and the film radius a [3,5,6,8–12]. When the film is spherical,

$$\frac{h_{\text{crit}}}{R} \sim (A_{H,\text{eff}}^*)^{2/5}, \quad (1.4)$$

where $A_{H,\text{eff}}^*$ is a dimensionless effective Hamaker constant $A_{H,\text{eff}}^* = A'_{H,\text{eff}}/\gamma R^2$. The critical film thickness for rupture when the film is dimpled, on the other hand, is

$$\frac{h_{\text{crit}}}{R} \sim (A_{H,\text{eff}}^*)^{1/3} \text{Ca}^{1/6}. \quad (1.5)$$

It follows that if $h_{\text{crit}} > h_{\text{trans}}$, the drainage time will scale as (1.3). On the other hand, if $h_{\text{crit}} \ll h_{\text{trans}}$, the observable scaling will follow (1.2). Between these limiting cases, there will be a transition between (1.2) and (1.3). Utilizing (1.4), we see that the criterion $h_{\text{crit}} > h_{\text{trans}}$ becomes

$$\beta_2 \text{Ca} < \left(\frac{A'_{H,\text{eff}}}{\gamma R^2} \right)^{2/5}. \quad (1.6)$$

We see that the scaling (1.3) is favored for small capillary numbers, with the allowable range increasing as the drop size decreases. We can also write (1.6) in the form

$$R < \left(\frac{A'_{H,\text{eff}}}{\gamma} \right)^{1/2} \left(\frac{1}{\beta_2 \text{Ca}} \right)^{5/4}. \quad (1.7)$$

In other words, the scaling (1.3) is relevant for small drops and the required size goes down as the strain rate goes up.

Systematic experimental studies of drainage of the film between two identical drops colliding head on in a compressional flow have been performed using the four-roll mill by Leal [1]. These experiments [2,5] indicate that for large capillary numbers, the drainage time prior to coalescence

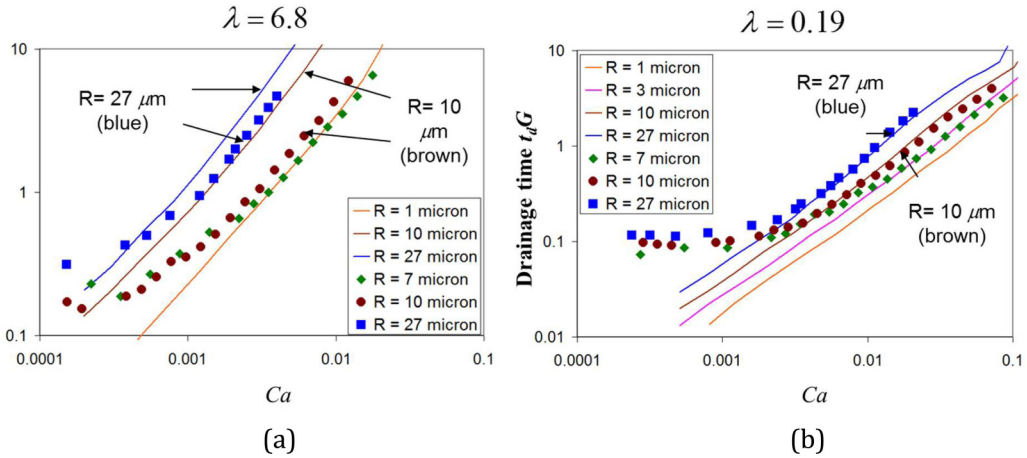


FIG. 1. Variation of the normalized drainage time $t_d G$ with the capillary number Ca for two different viscosity ratios (a) $\lambda = 6.8$ and (b) $\lambda = 0.19$. The symbols represent the experimental data of Hsu *et al.* [3], while the curves are the simulations of Yoon *et al.* [5].

obeys the relationship (1.1) for drops above $27 \mu\text{m}$ in size. This relationship was verified for different viscosities of the drop and suspending fluids and for different drop radii (greater than $27 \mu\text{m}$).

At low capillary numbers, the trends from the Yang *et al.* [4] experiments were unclear due to the scatter in the data. However, the simulations of Janssen *et al.* [6] and Yoon *et al.* [5] confirmed the expectation that if the capillary numbers were small, the film would be predominantly spherical during the drainage process up to the point of coalescence. Hsu *et al.* [3] set out to test the theoretical predictions of Janssen *et al.* [6] and Yoon *et al.* [5] by performing experiments with much smaller droplets than Yang *et al.* [4], ranging in size from 7 to $27 \mu\text{m}$. They demonstrated that for these small drops, there indeed exists a regime where the exponent m always lies in the range $1 < m < 4/3$, irrespective of the viscosity ratio. The value of m was closer to 1 for the small $7\text{-}\mu\text{m}$ drops and closer to $4/3$ for the larger $27\text{-}\mu\text{m}$ drops. However, a serious discrepancy they noted was that the measured drainage times were shorter than the values expected from the simulations of Yoon *et al.* [5]. This can be seen in Fig. 1, where we have compared the drainage times from experiment and simulations. The discrepancy is significant for high viscosity ratios and small drops. For example, for $R = 10 \mu\text{m}$ and $\lambda = 6.8$ [see Fig. 1(a)], the experimentally measured value of $t_d G$ is about 3 , while the simulations predict a value of about 9 , an error of 200% . Even for a low viscosity ratio of $\lambda = 0.19$ [see Fig. 1(b)], the overprediction is significant for small drops. For example, the experimental data for the $7\text{-}\mu\text{m}$ drops overlap with the theoretical prediction for $3\text{-}\mu\text{m}$ drops at high capillary numbers.

These discrepancies suggest that the theory and its underlying assumptions need to be revisited. From the data of Yoon *et al.* [5] (Fig. 19 of their paper), one can see that the minimum separation between the drops before the film becomes unstable can be over three orders of magnitude smaller than the drop radius. Therefore, for $1\text{-}\mu\text{m}$ drops, the critical film thickness can be as low as 1 nm . For such length scales, it is unreasonable to expect the continuum approximation, upon which the theory is based, to remain valid. Perhaps, the first assumption that is likely to break down as the film approaches such thicknesses is the boundary condition imposed at the interface.

In the theory, the interface is assumed to be a line of zero thickness that obeys the no-slip condition, i.e., the tangential velocity at the boundary is assumed to be continuous across the interface. However, the liquids employed in the experimental work cited above are polymers and it is well known that the interface between two different polymers is diffuse in nature due to the incompatibility of the two polymers. Furthermore, if the polymers have low entanglement densities in this interfacial region but are highly entangled in the bulk phase, the viscosity of the interfacial region can be orders of magnitude smaller than the bulk phase viscosities. Thus, even though the interface is extremely thin

(~ 1 nm), the large viscosity contrast ascribes to the interface a significant slip. As explained in a previous publication [13,14], to account for interfacial slip, we continue to treat the interface as a line of zero thickness, but replace the no-slip boundary condition at the interface with the Navier slip boundary condition characterized by a slip coefficient α' . If the viscosity of the diffuse region is much lower than either of the bulk viscosities, then α' can be approximated as [13]

$$\alpha' = \frac{d_I}{\mu_I}. \quad (1.8)$$

Here d_I and μ_I are the thickness and the inverse of the average mobility, respectively, of the interfacial region and can be predicted using the theories of Helfand and Tagami [15] and Goveas and Fredrickson [16]. Note that invoking the Navier slip condition essentially assumes that the slip velocity is directly proportional to the shear stress. Prior experimental studies from Macosko *et al.* [17] involving coextrusion of multiple alternating layers of polystyrene and polypropylene have revealed that the slip velocity is a stronger function of shear stress, with an exponent of 6.2 for stresses in the range of 1–10 kPa and an exponent of 1.8 for stresses exceeding 10 kPa. The stresses corresponding to film drainage are about 100 Pa or smaller, a regime in which the Macosko *et al.* [17] was unable to measure significant slip. However, recent careful measurements by Wagner [18] have shown that the slip velocity is indeed proportional to the shear stress for low magnitudes of stresses.

Besides the argument in the previous paragraph of breakdown of the continuum approximation, there have already been studies that indicate that slip increases the rate of drainage of the fluid. In a careful investigation, Park *et al.* [12] showed that for fixed capillary number, viscosity ratio, and drop radius, increasing the molecular weight of the fluids leads to a decrease in the normalized drainage time, particularly for large molecular weight fluids. They also showed that the reduction in the drainage time at high molecular weights was suppressed when a diblock copolymer was introduced at the interface as a compatibilizer, due to the fact that the copolymer spans the diffuse region and mitigates the incompatibility. However, in the Park *et al.* [12] and Hsu *et al.* [3] studies, the exact mechanisms of how interfacial slip affects the drainage process, and the parameter regimes where the effect of slip is maximized, were not identified.

In this paper we show that interfacial slip can account not only for the reduced drainage time observed in the experiments for the small viscous drops, but also for the observation in Fig. 1 that the power-law index of the $t_d G$ vs Ca behavior for higher Ca is reduced for smaller drops. We revisit the earlier analyses of Park *et al.* and Hsu *et al.* to identify the expected scaling of the drainage time with capillary number in the slip-dominant regime. The important change we introduce to their analysis is the employment of the correct scaling for the film pressure gradient in the dimpled-film regime, as suggested in Ref. [7]. The analysis elucidates six modes of drainage of the film, with the drainage times and critical capillary numbers for transition from one mode to another. The scaling analysis eventually leads to the drainage time vs capillary number relationships in the limits where slip is important, along with the combinations of Ca , slip coefficient, and dimensionless Hamaker constant where these regimes exist.

II. SCALING ANALYSIS

In this section we implement a scaling analysis for the drainage time for a spherical or dimpled film between two drops of radius R undergoing a head-on collision. As shown in Fig. 2, the drops are pushed against each other by an ambient, uniaxial compressional flow characterized by strain rate G ,

$$\mathbf{u}_\infty = \left[\frac{1}{2}x, \frac{1}{2}y, -z \right]. \quad (2.1)$$

We assume that the suspending and drop fluids are two Newtonian fluids, with viscosities μ and $\hat{\mu} = \lambda\mu$, respectively, and that they are separated by a deformable interface with an interfacial tension γ .

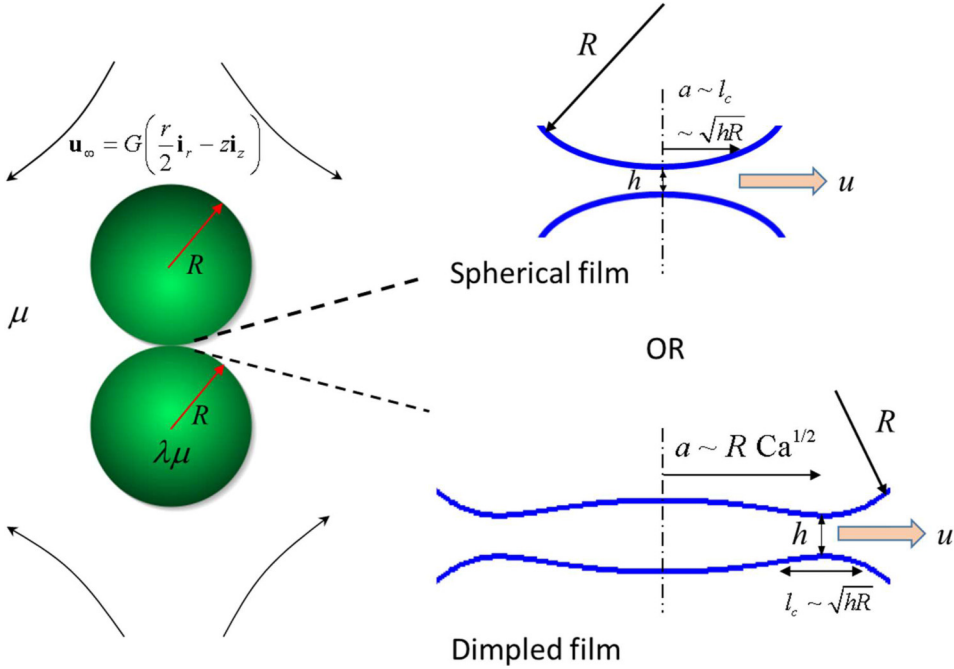


FIG. 2. Schematic of the axisymmetric head-on collision between two drops of the same radius R . The suspending fluid viscosity is μ , while the drop viscosity is $\lambda\mu$, where λ is the viscosity ratio. The ambient velocity field \mathbf{u}_∞ is a uniaxial compressional flow.

The rate of thinning of the film of thickness h between the drops is given by a mass balance

$$\frac{dh}{dt} \sim -\frac{h}{a}u, \quad (2.2)$$

where a is the radius of the film and u is the characteristic velocity of efflux of fluid (at $r = a$) in the region of thickness h , as depicted in Fig. 2. The efflux velocity comprises two parts, a pressure-driven parabolic component u_p and a tangential component u_t ,

$$u = u_t + u_p. \quad (2.3)$$

The parabolic component is estimated using lubrication theory as

$$u_p \sim \frac{h^2}{\mu} \frac{\gamma/R}{l_c}. \quad (2.4)$$

Here l_c is the length scale over which the pressure drop occurs in the film and depends on the shape of the film.

To determine the tangential velocity, we equate the tangential stress τ at the interface between the drop and the fluid inside the drops:

$$\tau \sim \frac{\mu u_p}{h} \sim \frac{\hat{\mu} \hat{u}_t}{l_c}, \quad (2.5)$$

where \hat{u}_t is the tangential velocity of the drop fluid. This stress balance assumes that the flow in the drop is influenced only by the film drainage process and is unaffected by the external flow (see, e.g., [19]). The tangential velocity within the thin film and inside the drop are related by the Navier slip

condition

$$u_t \sim \hat{u}_t + \alpha\tau \sim \hat{u}_t + \alpha' \left(\frac{\mu u_p}{h} \right). \quad (2.6)$$

Substituting for \hat{u}_t from Eq. (2.5) we have

$$u_t \sim \hat{u}_t + \alpha\tau \sim \frac{l_c u_p}{\lambda h} + \alpha' \left(\frac{\mu u_p}{h} \right) = u_p \left(\frac{l_c}{\lambda h} + \frac{\alpha' \mu}{h} \right). \quad (2.7)$$

The total velocity in the film can be obtained by substituting Eq. (2.7) into Eq. (2.3),

$$u \sim u_p \left(1 + \frac{l_c}{\lambda h} + \frac{\alpha' \mu}{h} \right). \quad (2.8)$$

The length scale l_c for both spherical (see, e.g., [3,6]) and dimpled films [7] can be shown to scale as

$$l_c \sim \sqrt{hR}. \quad (2.9)$$

The adoption of \sqrt{hR} as the length scale for the gradient of the pressure difference in the dimpled-film regime, rather than the film radius $a \sim R \text{Ca}^{1/2}$ as has often been done in the past by assuming a flat film [3–6,8–12], is a key difference between this and prior analyses of the drainage process. As we will see later, it not only leads to the experimentally observed scaling for the drainage time in the dimpled-film regime (as also noted by Frostad *et al.* [7]), but also the correct scaling for the critical capillary number for hindrance of coalescence in a head-on collision. Substituting for l_c in Eq. (2.8) yields

$$u \sim u_p \left(1 + \frac{1}{\lambda} \sqrt{\frac{R}{h}} + \frac{\alpha' \mu}{h} \right). \quad (2.10)$$

The above expression can be substituted back into Eq. (2.2) to get the film drainage rate

$$\frac{dh}{dt} \sim -\frac{h}{a} u_p \left(1 + \frac{1}{\lambda} \sqrt{\frac{R}{h}} + \frac{\alpha' \mu}{h} \right), \quad (2.11)$$

which, using Eqs. (2.4) and (2.9), can be further simplified to

$$\frac{dh}{dt} \sim -\frac{h^{3/2}}{\lambda\mu} \frac{\gamma}{aR^{1/2}} \left(\lambda \frac{h}{R} + \sqrt{\frac{h}{R}} + \frac{\alpha' \lambda \mu}{R} \right), \quad (2.12)$$

where the terms in parentheses denote the parabolic, tangential, and slip components, respectively.

Equation (2.12) is the basic equation of film drainage. In the above equation, the shape of the film appears only in the form of the film radius a in the prefactor. One immediately notes that any nonzero value of the slip coefficient leads to an increase in dh/dt . Thus, slip *always* accelerates the drainage process. The expression in the parentheses is comprised of three terms: the pressure-driven parabolic component, the tangential component, and the slip component. The relative magnitude of these terms depends on the dimensionless film thickness h/R but not the shape of the film.

We can identify three critical values for h/R . The first is

$$\frac{h_{c_1}}{R} = \lambda^{-2}. \quad (2.13)$$

The critical film thickness h_{c_1}/R marks the point where the tangential contribution to (2.12) exceeds the parabolic contribution. In particular, if

$$\frac{h_{c_1}}{R} \ll \frac{h}{R} \ll 1,$$

the parabolic component of the velocity profile is dominant over the tangential component, whereas if

$$\frac{h}{R} \ll \frac{h_{c_1}}{R},$$

the tangential component is dominant. Of course, we assume in all cases that $h/R \ll 1$ is consistent with the fact that we have a thin film. However, h_{c_1}/R is only small if $\lambda \gg 1$. Hence, the parabolic contribution to the film drainage process can only play a significant role if $\lambda \gg 1$. More often (i.e., when λ is not very large), the tangential component in Eq. (2.12) will be larger than the parabolic component.

The other critical values for h/R are

$$\frac{h_{c_2}}{R} = \alpha, \quad \frac{h_{c_3}}{R} = \alpha^2 \lambda^2 = \frac{h_{c_2}^2}{h_{c_1} R}, \quad (2.14)$$

where α is the dimensionless slip coefficient

$$\alpha = \frac{\alpha' \mu}{R}. \quad (2.15)$$

These two values for the critical film thickness demarcate the points when the slip component in Eq. (2.12) is comparable to the other two terms. Specifically, h_{c_2}/R is the film thickness when the slip component has the same magnitude as the parabolic component and h_{c_3}/R is the film thickness when the slip component has the same magnitude as the tangential component.

For purposes of future discussion, we will identify the situation in which $h_0 > h_{c_1}$ as case 1 and that in which $h_0 < h_{c_1}$ as case 2. It is further convenient to identify the regimes where one of the three terms in Eq. (2.12) is dominant: We will refer to the regime where the parabolic term is dominant ($h \gg h_{c_1}$) as limit 1, the regime where the tangential term is dominant ($h_{c_3} \ll h \ll h_{c_1}$) as limit 2, and the regime where the slip component is dominant as limit 3. In the latter case, we may also wish to distinguish case 1, where $h > h_{c_1}$ and the transition to dominant slip occurs when $h \ll h_{c_2}$, from case 2, where $h < h_{c_1}$ and the transition occurs when $h \ll h_{c_3}$. We will refer to the former case as limit 3a and the latter as limit 3b.

For case 1, we introduce the dimensionless ratio of the critical film thicknesses h_{c_2} and h_{c_1} :

$$\delta = \frac{h_{c_2}}{h_{c_1}} = \alpha \lambda^2.$$

The magnitude of δ determines when the slip term comes into play relative to the transition from the parabolic to the tangential velocity component in Eq. (2.12). If $\delta \ll 1$, which occurs for small slip coefficients and large drop radii, drainage initially occurs in limit 1 since $h_0 > h_{c_1}$, then transitions to limit 2 when $h_{c_3} \ll h \ll h_{c_1}$, and finally ends up in limit 3b for $h \ll h_{c_3}$. On the other hand, if $\delta \gg 1$, drainage occurs first in limit 1, but then transitions directly to limit 3a when $h \ll h_{c_2}$. Limit 2 is absent in this case. These two possibilities are schematically represented in Fig. 3.

In the more common situation, which we termed case 2, $h_0 < h_{c_1}$, the tangential term is dominant over the parabolic term throughout the drainage process. We note that this will always be the case when $\lambda \leq O(1)$ since then $h_{c_1}/R > O(1)$, while the condition that the film is thin requires $h/R \ll 1$. In case 2, the drainage process generally starts in limit 2 (assuming $h_0 > h_{c_3}$) and then proceeds to limit 3b when $h \ll h_{c_3}$.

The drainage regimes, as discussed above, represent only the fluid dynamic picture. Furthermore, they are independent of the shape of the film, i.e., whether it is spherical or dimpled. However, the modes that will actually manifest in either case 1 or case 2 depend on the initial film thickness at contact h_0 and the critical film thickness h_{crit} for film rupture, which serve as a start and a stop, respectively, for the drainage process, as well as the slip coefficient α' , which is needed to determine when slip is important. As noted earlier, we can use the theories of Helfand and Tagami [15] and Goveas and Fredrickson [16] to evaluate the slip coefficient. If we focus on the

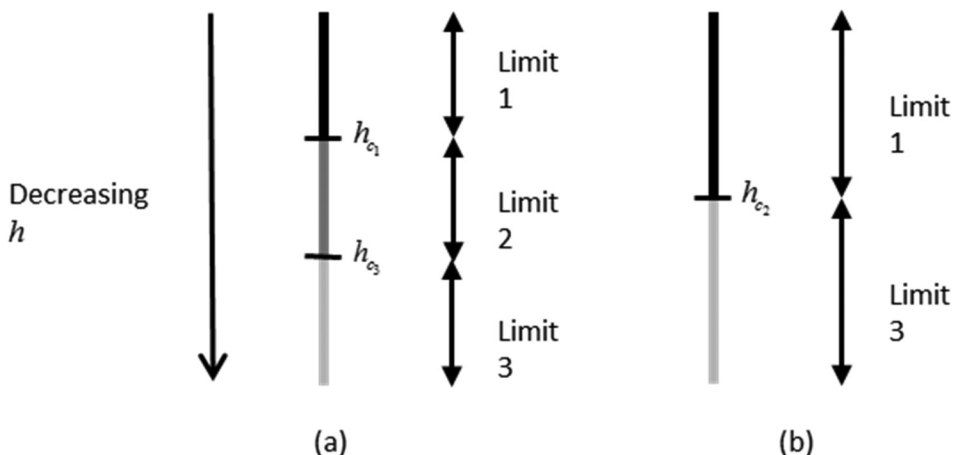


FIG. 3. Schematic representation for case 1 ($h_0 > h_{c1}$) of the various limits of the drainage process for (a) $\delta \ll 1$ and (b) $\delta \gg 1$ ($\delta = \alpha\lambda^2$): limit 1, the fluid efflux in the film is dominated by the Laplace pressure difference component; limit 2, the film efflux is dominated by the contribution of the tangential velocity of the interface; and limit 3, the film efflux is dominated by the interfacial slip component. Limit 1 will be observed for thin films only for viscosity ratios much greater than unity.

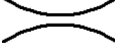
combination of polymers polydimethylsiloxane (PDMS) and polybutadiene (PBd), which was used in the experiments of Park *et al.* [12] and Hsu *et al.* [3], we can show that d_I and μ_I are 0.564 nm and 0.02 Pa s, respectively (see [12] for details). The slip coefficient $\alpha' = d_I/\mu_I$ for the PDMS-PBd combination is therefore 2.5×10^{-8} SI units. If we consider suspending fluid viscosities ranging from 1 to 100 Pa s and drop radii ranging from 1 to 100 μm (see, e.g., [13]), the dimensionless slip coefficient (2.15) can vary from about 10^{-4} to 1.

We can see that the drainage regime will depend on whether $h_0 > h_{c1}$ or $h_0 < h_{c1}$, i.e., whether we follow the drainage protocols of case 1 or case 2. In case 1, $h_0 > h_{c1}$ and the basic question is the magnitude of h_{crit} compared to h_{c1} and h_{c3} for $\delta \ll 1$ and compared to h_{c2} for $\delta \gg 1$. If we refer again to Fig. 3, we can see that h_{crit} determines where in the transition from one limit to another the film ruptures. For case 2, on the other hand, the film is dominated by the tangential velocity component from the beginning and the slip transition occurs for $h = O(h_{c3})$. The magnitude of h_{crit} then determines whether the film ruptures before this transition or after. If $h_{c3} < h_{\text{crit}}$ the film will rupture before the slip component becomes significant, while if $h_0 > h_{c3}$ the film will drain for some time without slip before the slip component comes into play.

With knowledge of the film radius, the critical film thickness, and the capillary number, we can calculate the drainage time, assuming that drainage takes place entirely within one of the limiting cases when (2.12) is dominated by one of the three components of the velocity profile, from some initial film thickness for that regime until rupture. These results are presented in Table I. The table presents six different possible regimes of drainage: $S1$, $S2$, and $S3$ corresponding to the spherical film in limits 1, 2, and 3 respectively, and $D1$, $D2$, and $D3$ for dimpled films in the same three limits.

Several features of the drainage process are elucidated by Table I. First, we observe that for drainage in any one of the limits 1–3, for fixed capillary number, the spherical film drains faster than the dimpled film. Although l_c and thus the pressure gradients in the two cases are similar, the rate of decrease of the film thickness is smaller in the case of the dimpled film simply because a larger volume of fluid needs to be removed in order for the film to thin. Second, for fixed initial and final film thicknesses h_i and h_f , respectively, the capillary number dependence of the drainage time depends only on the film shape: Ca^1 for spherical films and $\text{Ca}^{3/2}$ for dimpled films. In particular, we observe that for the dimpled film, the exponents for the cases where slip is absent ($D1$ and $D2$) is the same as for the case where slip is dominant ($D3$) (an index of $3/2$). This is in contrast with

TABLE I. Results of the scaling analysis for spherical and dimpled films.

	Spherical film	Dimpled film
shape		
l_c	\sqrt{hR}	\sqrt{hR}
a	\sqrt{hR}	$R \text{Ca}^{1/2}$
h_{crit}	$h_{\text{crit}} \sim R(A_{H,\text{eff}}^*)^{2/5}$	$h_{\text{crit}} \sim R(A_{H,\text{eff}}^*)^{1/3} \text{Ca}^{1/6}$
	Regime S1	Regime D1
$t_d G$ in limit 1 (film drainage is dominated by the pressure-driven component)	$(tG)_{S1} \sim \text{Ca} \left[\left(\frac{h_f}{R} \right)^{-1} - \left(\frac{h_i}{R} \right)^{-1} \right]$ For $h_f = h_{\text{crit}} \ll h_i$, $(t_d G)_{S1} \sim \text{Ca} (A_{H,\text{eff}}^*)^{-2/5}$, or $(t_d G)_{S1} \propto R^{4/5} \text{Ca}$	$(tG)_{D1} \sim \text{Ca}^{3/2} \left[\left(\frac{h_f}{R} \right)^{-3/2} - \left(\frac{h_i}{R} \right)^{-3/2} \right]$ For $h_f = h_{\text{crit}} \ll h_i$, $(t_d G)_{D1} \sim \text{Ca}^{3/2} (A_{H,\text{eff}}^*)^{-1/2}$, or $(t_d G)_{D1} \propto R \text{Ca}^{3/2}$
	Regime S2	Regime D2
$t_d G$ in limit 2 (film drainage is dominated by the tangential velocity)	$(tG)_{S2} \sim \lambda \text{Ca} \left[\left(\frac{h_f}{R} \right)^{-1/2} - \left(\frac{h_i}{R} \right)^{-1/2} \right]$ For $h_f = h_{\text{crit}} \ll h_i$, $(t_d G)_{S2} \sim \lambda \text{Ca} (A_{H,\text{eff}}^*)^{-1/5}$, or $(t_d G)_{S2} \propto \lambda R^{2/5} \text{Ca}$	$(tG)_{D2} \sim \lambda \text{Ca}^{3/2} \left[\left(\frac{h_f}{R} \right)^{-1} - \left(\frac{h_i}{R} \right)^{-1} \right]$ For $h_f = h_{\text{crit}} \ll h_i$, $(t_d G)_{D2} \sim \lambda \text{Ca}^{4/3} (A_{H,\text{eff}}^*)^{-1/3}$, or $(t_d G)_{D2} \propto \lambda R^{2/3} \text{Ca}^{4/3}$
	Regime S3	Regime D3
$t_d G$ in limit 3 (film drainage is dominated by interfacial slip)	$(tG)_{S3} \sim \frac{1}{\alpha} \text{Ca} \ln \left(\frac{h_i}{h_f} \right)$ For $h_f = h_{\text{crit}}$, $(t_d G)_{S3} \sim \frac{1}{\alpha} \text{Ca} \ln \left(\frac{h_i}{R(A_{H,\text{eff}}^*)^{2/5}} \right)$	$(tG)_{D3} \sim \frac{1}{\alpha} \text{Ca}^{3/2} \left[\left(\frac{h_f}{R} \right)^{-1/2} - \left(\frac{h_i}{R} \right)^{-1/2} \right]$ For $h_f = h_{\text{crit}} \ll h_i$, $(t_d G)_{D3} \sim \frac{1}{\alpha} \text{Ca}^{17/12} (A_{H,\text{eff}}^*)^{-1/6}$, or $(t_d G)_{D3} \propto R^{4/3} \text{Ca}^{17/12}$

the scaling analysis of Hsu *et al.* [3], which predicts a significantly different exponent of 2 in the slip-dominant case. The change has come about due to the employment of the correct scaling for the pressure gradient in the dimpled film, as elucidated by Frostad *et al.* [7]. This would imply that if the dominant shape of the film during the drainage process remains dimpled, there should not be a significant change in the exponent m as one transitions from the no-slip regime to the slip-dominant regime, by increasing, for example, the slip coefficient. Although the Ca dependence is the same for the same film shape, the functional dependence of the drainage time on the film height becomes weaker, i.e., the film drains faster, as one progresses from limit 1 to limit 3.

In the following section we will employ the results in Table I along with the various critical heights pointed out in this section to elucidate various modes of drainage with interfacial slip.

III. MODES OF FILM DRAINAGE

The scaling analysis presented in the previous section revealed five critical values of the film thickness: h_{c1} , h_0 , h_{trans} , h_{crit} , and either h_{c2} or h_{c3} , the latter depending on whether the parabolic or tangential component of velocity is dominant when the transition to the slip component takes place. Out of these various film thicknesses, only two depend on the imposed strain rate G : the initial thickness h_0 and the spherical-dimple transition thickness h_{trans} [h_{crit} depends on the capillary number in the dimpled-film regime, but only very weakly (1/6 power)]. As G (or Ca) is increased, both h_0 and h_{trans} increase proportionately and $h_0 > h_{\text{trans}}$ for all Ca. The values of these two film thicknesses relative to the other critical film thicknesses determine the dynamics of the drainage process as a function of the capillary number. Here we will consider some asymptotic limits to elucidate the various modes of drainage. However, for brevity, we restrict ourselves to the case when the initial film thickness h_0 is small enough to avoid case 1 (i.e., $h_0 < h_{c1}$); this is generally valid for

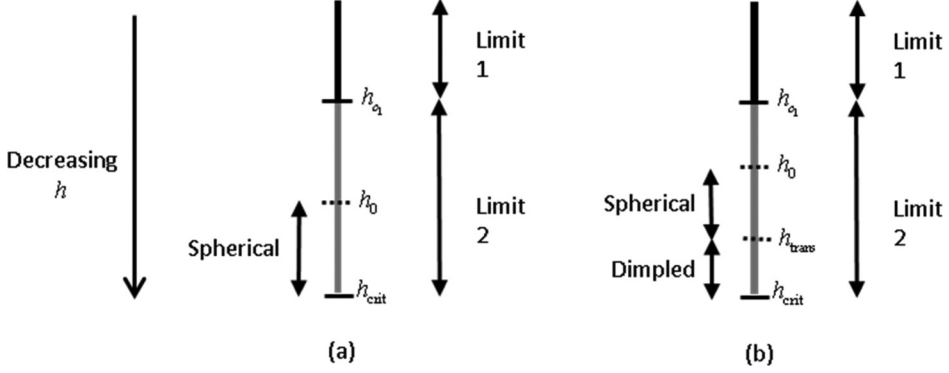


FIG. 4. The two drainage modes (a) $S2$ and (b) $S2 \rightarrow D2$ for situation A for $h_0 < h_{c1}$.

the small capillary numbers and is always true if the viscosity ratio $\lambda = O(1)$. In this case, we need only concern ourselves with h_{c1} , h_0 , h_{trans} , h_{crit} , and h_{c3} . It is straightforward to extend the analysis below to include case 1.

A. Situation A: $h_0 > h_{\text{crit}} > h_{c3}$

This asymptotic limit is essentially that of no slip, because the critical film thickness for rupture is greater than the height h_{c3} , below which the effects of slip (limit 3) can be observed. As shown schematically in Fig. 4, two modes of drainage can be observed as the strain rate is increased. For small strain rates $h_0 > h \geq h_{\text{crit}} > h_{\text{trans}}$, the film is purely spherical in shape ($S2$) throughout the drainage process. However, for higher strain rates $h_0 > h \geq h_{\text{trans}} > h_{\text{crit}}$, the film is spherical initially ($h > h_{\text{trans}}$), but transitions to a dimpled shape ($S2 \rightarrow D2$) before finally rupturing when $h = h_{\text{crit}}$. (Due to our restriction on h_0 , both modes occur in case 2; case 1 is not approached.) These two limits have been observed in both theoretical calculations [5,6] and experiments [2–4]. The transition from the $S2$ mode to the $S2 \rightarrow D2$ mode occurs when $h_{\text{trans}} \sim h_{\text{crit}}$. We have previously seen that $h_{\text{crit}} \sim R(A_H^*)^{2/5}$ for spherical films (also see Table I), while $h_{\text{trans}} = \beta_2 R \text{Ca}$. It follows that the capillary number that separates the $S2$ and $S2 \rightarrow D2$ modes is

$$\text{Ca}_c \sim (A_H^*)^{2/5}. \quad (3.1)$$

An alternative way of estimating this transition condition is to compare the drainage times in the two modes. For the mode $S2$, the drainage time is

$$(tG)_{\text{mode } S2} \approx \lambda \text{Ca} (A_{H,\text{eff}}^*)^{-1/5}, \quad (3.2)$$

while for the mode $S2 \rightarrow D2$,

$$(tG)_{\text{mode } S2 \rightarrow D2} |_{\text{Ca} \gg 1} \approx \lambda \text{Ca}^{4/3} (A_{H,\text{eff}}^*)^{-1/3}. \quad (3.3)$$

In the asymptotic limit of small capillary numbers, the film drainage time is dominated by $(t_d G)_{S2}$ (see Table I), while for higher capillary numbers, it is controlled by the time $(t_d G)_{D2}$, corresponding to the $D2$ phase, since dimpled films drain slower than spherical films in the same limit. These two limits will overlap at that capillary number for which $(t_d G)_{S2} \sim (t_d G)_{D2}$ and this condition, using the results in Table I, yields the capillary number for transition, once again, as $\text{Ca} \sim (A_H^*)^{2/5}$.

These results suggest that if we plot the drainage time data using the normalized coordinates $\text{Ca}/(A_{H,\text{eff}}^*)^{2/5}$ and $t_d G/(A_{H,\text{eff}}^*)^{1/5}$, the data belonging to these two modes will collapse onto a single master curve. In Fig. 5 we show the raw data of $t_d G$ vs Ca from the simulations of Yoon *et al.* [5] in the left column for three viscosity ratios $\lambda = 0.19, 1.2,$ and 6.8 and the same data in the normalized coordinates in the right column. We see that the data for each viscosity ratio fall on a

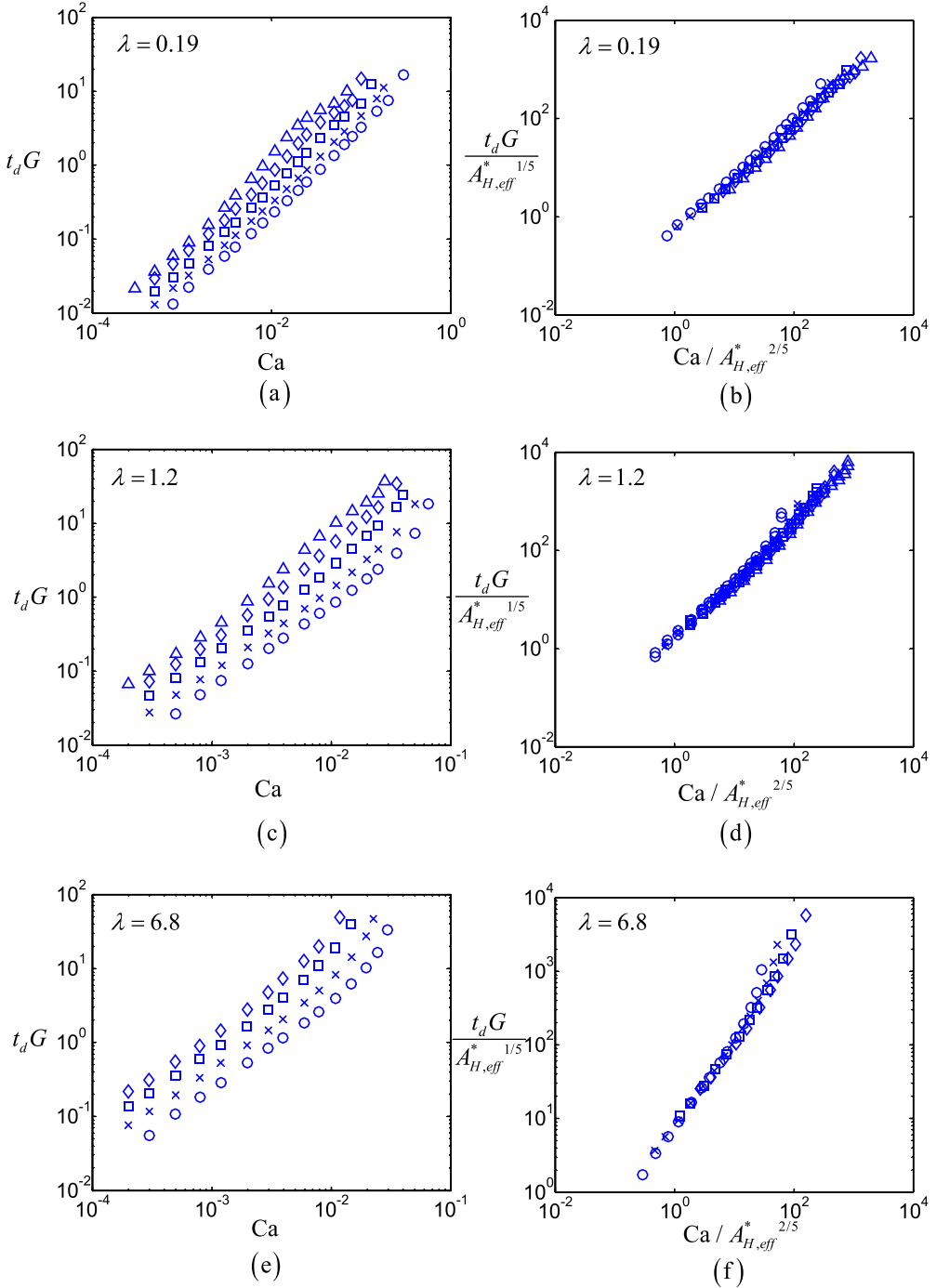


FIG. 5. (a), (c), and (e) Variations of the dimensionless drainage with the capillary number ($t_d G$ vs Ca) and (b), (d), and (f) the normalized drainage time with the normalized capillary number [$t_d G / (A_{H,eff}^*)^{1/5}$ vs $Ca / (A_{H,eff}^*)^{2/5}$] for three different viscosity ratios (a) and (b) $\lambda = 0.19$, (c) and (d) $\lambda = 1.2$, and (e) and (f) $\lambda = 6.8$: circles, $R = 1 \mu\text{m}$; crosses, $R = 3 \mu\text{m}$; squares, $R = 10 \mu\text{m}$; diamonds, $R = 27 \mu\text{m}$; and triangles, $R = 70 \mu\text{m}$. The interfacial tensions used in these calculations were $\gamma = 4.6, 4.8,$ and 5.0 mN/m for $\lambda = 0.19, 1.2,$ and 6.8 , respectively. The Hamaker constant was taken as $A_{H,eff} = 3.199 \times 10^{-21} \text{ J}$.

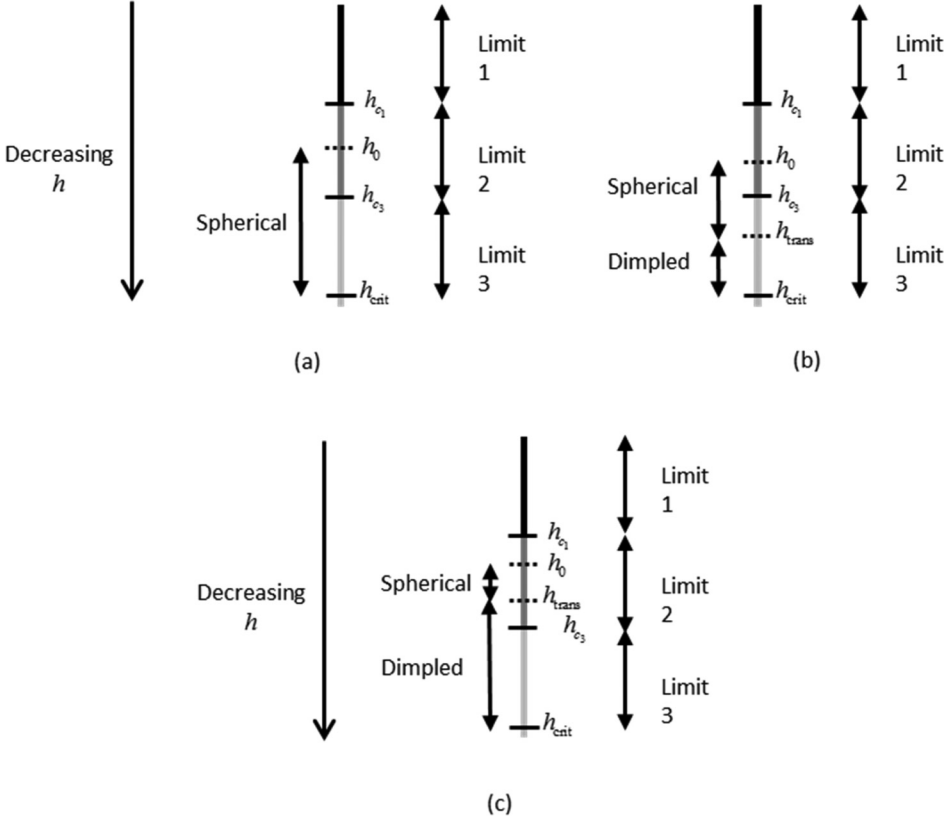


FIG. 6. The three possible drainage modes (a) $S2 \rightarrow S3$, (b) $S2 \rightarrow S3 \rightarrow D3$, and (c) $S2 \rightarrow D2 \rightarrow D3$ for situation B for $h_0 < h_{c1}$.

single master curve. There are some deviations from the master curves for higher capillary numbers of each data set, because, for these capillary numbers, the drainage process enters a different regime, where the flow induced within the drop by the external flow starts to affect film drainage; this effect is not captured in our scaling analysis.

Our normalized coordinates differ slightly in the exponents of $A_{H,\text{eff}}^*$ when compared to the simulation results of Janssen *et al.* [6], who used $\text{Ca}/(A_{H,\text{eff}}^*)^{0.3}$ and $t_d G/(A_{H,\text{eff}}^*)^{0.15}$. They obtained these exponents by fitting the drainage time data for a single viscosity ratio $\lambda = 1$. However, we have deduced the exponents from a scaling analysis and, as is evident from Fig. 5, these coordinates work for all three viscosity ratios.

B. Situation B: $h_0 > h_{c3} > h_{\text{crit}}$

This asymptotic limit represents the case when slip can influence the drainage process. We must always begin with a spherical-film shape since h_0 is always larger than h_{trans} . Furthermore, since $h_0 > h_{c3}$, all of these cases begin in the regime $S2$. This regime corresponds to capillary numbers satisfying

$$\text{Ca} > \frac{(\alpha\lambda)^2}{\beta_1}. \quad (3.4)$$

There are three modes of drainage that can be observed in this case: $S2 \rightarrow S3$, $S2 \rightarrow S3 \rightarrow D3$, and $S2 \rightarrow D2 \rightarrow D3$. These are shown schematically in Fig. 6.

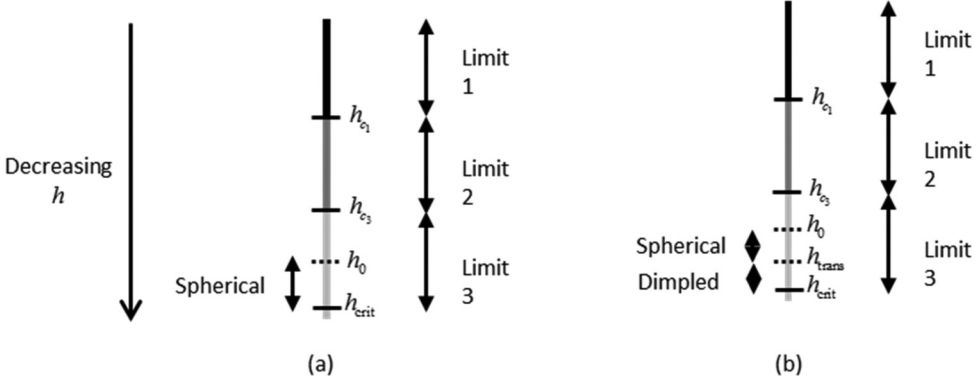


FIG. 7. The two possible drainage modes (a) $S3$ and (b) $S3 \rightarrow D3$ for situation C for $h_0 < h_{c3}$.

In the first case ($S2 \rightarrow S3$), $h_0 > h_{c3} > h_{crit} > h_{trans}$ and the film retains its spherical shape throughout the drainage process. However, in the other two cases, $h_{trans} > h_{crit}$ and there is a transition to a dimpled-film shape during the drainage process. In the case $S2 \rightarrow S3 \rightarrow D3$, the transition to slip occurs before the transition to a dimpled shape, i.e., $h_0 > h_{c3} > h_{trans} > h_{crit}$. On the other hand, in the case $S2 \rightarrow D2 \rightarrow D3$, the transition to a dimpled shape occurs prior to the onset of slip, i.e., $h_0 > h_{trans} > h_{c3} > h_{crit}$. The transition between these latter two cases occurs when $h_{trans} \sim h_{c3}$. This corresponds to a critical capillary number

$$Ca \sim \frac{(\alpha\lambda)^2}{\beta_2}. \quad (3.5)$$

For the highest viscosity ratio $\lambda = 6.8$ and the smallest drop size $R = 7 \mu\text{m}$ employed in our prior experiments, which would maximize the right-hand side of (3.5), this transition capillary number is about $O(10^{-3})$. This transition may be accessible in careful experiments.

C. Situation C: $h_{c3} > h_0 > h_{crit}$

In this situation, one can see that the entire drainage process will occur in limit 3. This situation can exist provided $h_0 < h_{c3}$, i.e., when

$$Ca < \frac{(\alpha\lambda)^2}{\beta_1}. \quad (3.6)$$

Given the estimate above for (3.5) and the fact that $\beta_1/\beta_2 = O(10)$, we can see that this regime will exist only for extremely small capillary numbers, less than $O(10^{-4})$, making its capture unlikely in the four-roll-mill experiments from our laboratory due to the extremely short drainage times.

There are two distinct cases, as shown in Fig. 7. In the first, where $h_{crit} > h_{trans}$, the drops remain spherical for the whole drainage process (i.e., drainage occurs in the limit $S3$), and in the second, where $h_{trans} > h_{crit}$, there is a transition ($S3 \rightarrow D3$) from a spherical-film shape to a dimpled one prior to rupture. The drainage time in mode $S3$ is (see Table I)

$$(t_d G)_{S3} \sim \frac{1}{\alpha} Ca \ln \left(\frac{\beta_1 Ca}{(A_{H,\text{eff}}^*)^{2/5}} \right). \quad (3.7)$$

We note that this is a stronger scaling with respect to Ca than the one derived for spherical films with no slip, where $t_d G \propto Ca$ [Eq. (1.3)].

The drainage process will transition from $S3$ to $D3$ with an increase in the capillary number so that h_{trans} is increased (see Fig. 8). As before, the transition between the two modes can be

obtained by equating the scalings for the drainage times in the $S3$ and $D3$ modes. Thus, by setting $(t_d G)_{S3} \sim (t_d G)_{D3}$ and using $h_i = h_0 = \beta_1 R Ca$, the critical capillary number marking the shift from mode $S3$ to mode $D3$ is

$$Ca_c \sim (\ln \beta_1)^{12/5} (A_{H,\text{eff}}^*)^{2/5}. \quad (3.8)$$

Interestingly, we see that the critical capillary numbers that mark the shift from a purely spherical mode to a purely dimpled mode of drainage in the no-slip limit [Eq. (3.1)] and the slip-dominant limit [Eq. (3.8)] scale exactly the same way with respect to the dimensionless Hamaker constant: $(A_{H,\text{eff}}^*)^{2/5}$. However, since $\beta_1 = O(10)$, the transition occurs at a higher value of capillary number in the slip-dominant case. Therefore, when comparing the $t_d G$ vs Ca curves for the no-slip and slip-dominant cases, all else remaining the same, we should anticipate a range of capillary numbers $(A_{H,\text{eff}}^*)^{2/5} < Ca < (\ln \beta_1)^{12/5} (A_{H,\text{eff}}^*)^{2/5}$ in which drainage occurs predominantly in the dimpled-film configuration for the no-slip case and predominantly in the spherical-film configuration for the slip-dominant case. We can also compare the drainage times in the slip-dominant regime and no-slip case for $Ca \gg Ca_c$. This ratio is

$$\frac{(t_d G)_{D3}}{(t_d G)_{D2}} \sim \frac{1}{\alpha \lambda} Ca^{1/12} (A_{H,\text{eff}}^*)^{1/6}, \quad (3.9)$$

which is a very weak function of Ca ($Ca^{0.083}$). Therefore, curves of $t_d G$ vs Ca with different slip coefficients should be nearly parallel to each other in the regime $Ca \gg Ca_c$.

IV. DISCUSSION

In the Introduction we noted two discrepancies between experiment and theory based on the no-slip boundary condition (see Fig. 1). First, the experimental drainage times are less than the theoretical ones and the difference becomes greater as the drops become smaller and more viscous relative to the suspending fluid. A more subtle difference is that while $t_d G$ vs Ca follows the expected $4/3$ power-law index based on the no-slip condition for large drops, this index becomes weaker for small drops and at high viscosity ratios [3]. The inclusion of slip can qualitatively account for both types of discrepancies. Slip makes the drainage process faster and the magnitude of the reduction depends on $\alpha \lambda = \alpha' \lambda \mu / R$ [see Eq. (2.12)]. For a given polymer-polymer combination (i.e., a fixed α'), large viscosity ratios and small drop radii will lead to an increased slip contribution to the total drainage rate, which is in agreement with the experimental trend. Examination of the experimental data, Table I, and the various regimes outlined in Sec. IV suggests that the regime that is likely observed for the capillary numbers explored in the experiments is $S2 \rightarrow S3$ or the transition between the $S2 \rightarrow S3$ and $S2 \rightarrow S3 \rightarrow D3$ regimes, for which the index of $t_d G$ with Ca is weaker than $4/3$.

The scaling analysis here is based on the case when the two drops are identical in radius. For two unequal drops of radii R_1 and R_2 , there is a simple modification to the results presented in this paper based on the work of Davis *et al.* [20]: replacement of drop radius R with the harmonic mean $R_1 R_2 / (R_1 + R_2)$.

In this scaling analysis, we have ignored the effect of the external flow on the flow inside the drop and in turn on the flow in the thin film. Prior work [5,17] has shown that for high capillary numbers, the drop-scale flow can arrest the drainage process, leading to hindrance of coalescence. For the drop scale flow to influence the flow within the film, the drop scale tangential stress τ_d imposed on the thin film should scale as the tangential stress τ in the film arising from the drainage process. The drop-flow-induced tangential stress τ_d imposed on the scale of the film radius is [17]

$$\tau_d \sim \lambda \mu G \left(\frac{a}{R} \right). \quad (4.1)$$

The usual values of the Hamaker constant, drop radius, and interfacial tensions typically lead to the drop-scale stress becoming important only in the dimpled regime. Therefore, employing

$a \sim R \text{Ca}^{1/2}$ (see Table I) in the above equation yields

$$\tau_d \sim \lambda \mu G \text{Ca}^{1/2}. \quad (4.2)$$

From Eqs. (2.4), (2.5), and (2.9) we can show that the stress in the film due to drainage τ scales as

$$\tau \sim \sqrt{\frac{h}{R}} \frac{\gamma}{R}. \quad (4.3)$$

Equating (4.1) and (4.2), we get the critical film thickness for transition into this regime as

$$\frac{h}{R} \sim \lambda^2 \text{Ca}^3. \quad (4.4)$$

In order for this regime to be observed, this thickness must be greater than the critical thickness of the film at rupture, which, from Table I, scales as

$$\frac{h_{\text{crit}}}{R} \sim (A_{H,\text{eff}}^*)^{1/3} \text{Ca}^{1/6} \quad (4.5)$$

for dimpled films. Thus, the critical capillary number for transition into the regime where coalescence is hindered in a head-on collision is

$$\text{Ca}_c \sim \lambda^{-12/17} (A_{H,\text{eff}}^*)^{2/17} \approx \lambda^{-0.71} (A_{H,\text{eff}}^*)^{0.12}. \quad (4.6)$$

This scaling is nearly identical to the analytical result derived by Yoon *et al.* [5] based on the work of Nemer *et al.* [17] [in fact, it would have been identical had we chosen the critical rupture thickness to be $h \sim R(A_{H,\text{eff}}^*)^{1/3}$]. This correct scaling has materialized due to the employment of the proper scaling for the pressure gradient length scale $l_c \sim \sqrt{h/R}$.

With the introduction of interfacial slip, the drop-scale flow-induced tangential stress τ_d is expected to decrease to [21]

$$\tau_d \sim \frac{\lambda}{1 + k\alpha\lambda} \mu G \left(\frac{a}{R} \right). \quad (4.7)$$

This will increase the critical capillary number to

$$\text{Ca}_c \sim (1 + k\alpha\lambda)^{12/7} \lambda^{-12/17} (A_{H,\text{eff}}^*)^{2/17}. \quad (4.8)$$

For large values of the slip coefficient, the critical capillary number becomes

$$\text{Ca}_c \sim \alpha^{12/7} (A_{H,\text{eff}}^*)^{2/17}, \quad (4.9)$$

which is independent of the viscosity ratio λ . Thus, while the critical capillary number for noncoalescence scales in exactly the same way with the dimensionless Hamaker constant as the no-slip case, the dependence on the viscosity ratio becomes weaker with an increase in α and the critical capillary number increases.

V. CONCLUSION

The scaling analysis based on the thin film approximation reveals that the introduction of interfacial slip will affect the curve of drainage time vs capillary number in five ways, which are summarized in Fig. 8. First, it will lead to a reduction in the drainage time. Second, it will result in a stronger scaling of $t_d G$ vs Ca in the spherical regime. Third, the scaling of $t_d G$ vs Ca in the dimpled regime will not be affected significantly. Fourth, slip will cause an increase in the magnitude of the critical capillary number for transition from the spherical to dimpled regime, but without a change in the scaling. Finally, slip is predicted to increase the critical capillary number for suppression of coalescence in a head-on collision; however, the scaling with the dimensionless Hamaker constant remains the same.

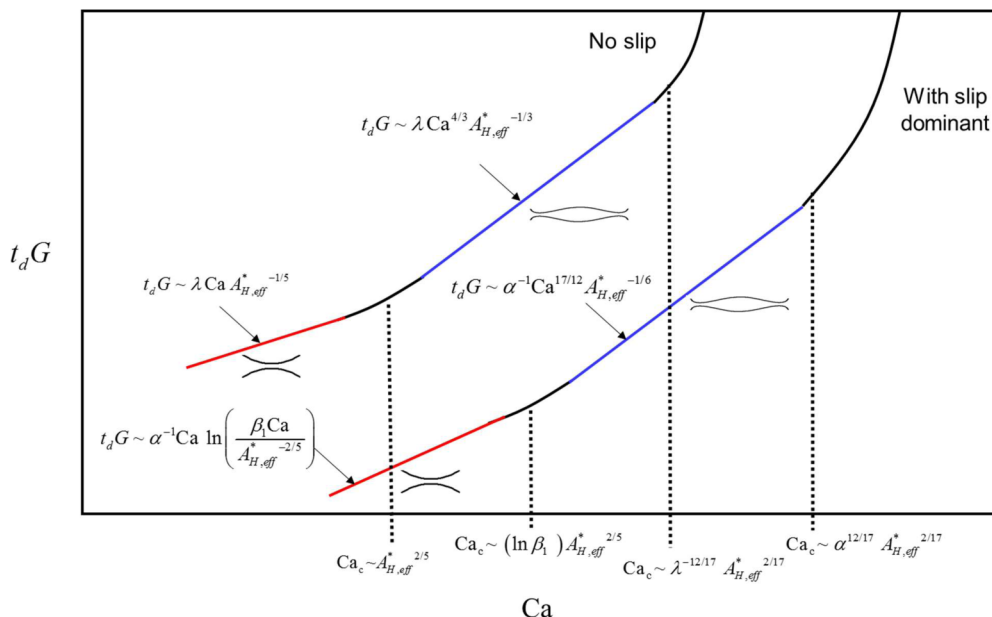


FIG. 8. Schematic of the variation of the drainage time with capillary number in the no-slip limit (top curve) and in the slip-dominant limit (bottom curve). (The changes in the slopes of the lines are exaggerated.)

ACKNOWLEDGMENT

A.R. acknowledges the Natural Sciences and Engineering Research Council of Canada Discovery Grant No. 402005 and the Ontario Early Researcher Award No. ER13-09-138 from the Ministry of Research and Innovation in Ontario.

-
- [1] L. G. Leal, Flow induced coalescence of drops in a viscous fluid, *Phys. Fluids* **16**, 1833 (2004).
 - [2] Y. Yoon, M. Borrell, C. C. Park, and L. G. Leal, Viscosity ratio effects on the coalescence of two equal-sized drops in a two-dimensional linear flow, *J. Fluid Mech.* **525**, 355 (2005).
 - [3] A. S. Hsu, A. Roy, and L. G. Leal, Drop-size effects on coalescence of two equal-sized drops in a head-on collision, *J. Rheol.* **52**, 1291 (2008).
 - [4] H. Yang, C. C. Park, Y. T. Hu, and L. G. Leal, The coalescence of two equal-sized drops in a two-dimensional linear flow, *Phys. Fluids* **13**, 1087 (2001).
 - [5] Y. Yoon, F. Baldessari, H. D. Ceniceros, and L. G. Leal, Coalescence of two equal-sized deformable drops in an axisymmetric flow, *Phys. Fluids* **19**, 102102 (2007).
 - [6] P. J. A. Janssen, P. D. Anderson, G. W. M. Peters, and H. E. H. Meijer, Axisymmetric boundary integral simulations of film drainage between two viscous drops, *J. Fluid Mech.* **567**, 65 (2006).
 - [7] J. M. Frostad, J. Walter, and L. G. Leal, A scaling relation for the capillary-pressure driven drainage of thin films, *Phys. Fluids* **25**, 052108 (2013).
 - [8] A. K. Chesters, The modeling of coalescence processes in fluid liquid dispersions—A review of current understanding, *Chem. Eng. Res. Des.* **69**, 259 (1991).
 - [9] A. Ajdari, Slippage at a polymer/polymer interface: Entanglements and associated friction, *C. R. Acad. Sci. Ser. II* **317**, 1159 (1993).
 - [10] N. P. Adhikari and J. L. Goveas, Effects of slip on the viscosity of polymer melts, *J. Polymer Sci. B* **42**, 1888 (2004).

- [11] F. Brochard-Wyart and P.-G. de Gennes, Sliding molecules at a polymer/polymer interface, *C. R. Acad. Sci. Ser. II* **317**, 13 (1993).
- [12] C. C. Park, F. Baldessari, and L. G. Leal, Study of molecular weight effects on coalescence: Interface slip layer, *J. Rheol.* **47**, 911 (2003).
- [13] A. Ramachandran, K. Tsigklifis, A. Roy, and G. Leal, The effect of interfacial slip on the dynamics of a drop in flow: Part I. Stretching, relaxation, and breakup, *J. Rheol.* **56**, 45 (2012).
- [14] A. Ramachandran and L. G. Leal, The effect of interfacial slip on the rheology of a dilute emulsion of drops for small capillary numbers, *J. Rheol.* **56**, 1555 (2012).
- [15] E. Helfand and Y. Tagami, Theory of the interface between immiscible polymers, *J. Chem. Phys.* **57**, 1812 (1972).
- [16] J. L. Goveas and G. H. Fredrickson, Apparent slip at a polymer-polymer interface, *Eur. Phys. J. B* **2**, 79 (1998).
- [17] R. Zhao and C. W. Macosko, Slip at polymer-polymer interfaces: Rheological measurements on coextruded multilayers, *J. Rheol.* **46**, 145 (2002); P. C. Lee, H. E. Park, D. C. Morse, and C. W. Macosko, Polymer-polymer interfacial slip in multilayered films, *ibid.* **53**, 893 (2009); H. E. Park, P. C. Lee, and C. W. Macosko, Polymer-polymer interfacial slip by direct visualization and by stress reduction, *ibid.* **54**, 1207 (2010).
- [18] T. Himmel and M. H. Wagner, Experimental determination of interfacial slip between polyethylene and thermoplastic elastomers, *J. Rheol.* **57**, 1773 (2013).
- [19] M. B. Nemer, X. Chen, D. H. Papadopoulos, J. Bławdziewicz, and M. Loewenberg, Hindered and Enhanced Coalescence of Drops in Stokes Flows, *Phys. Rev. Lett.* **92**, 114501 (2004).
- [20] R. H. Davis, J. A. Schonberg, and J. M. Rallison, The lubrication force between two viscous drops, *Phys. Fluids A* **1**, 77 (1989).
- [21] S. Goel and A. Ramachandran, Two touching spherical drops in a uniaxial compressional flow: The effect of interfacial slip, *Phys. Fluids* **28**, 053303 (2016).